# Analysis of the visualizing changes in radar time series using the REACTIV method through satellite imagery

**Hamood Shehab Hamid[1], Raad Farhood Chisab[2]**

[1]Department of Computer Engineering Techniques, Electrical Engineering Technical College, Middle Technical University, Baghdad, Iraq
[2]Department of Electrical Techniques, Technical Institute-Kut, Middle Technical University, Baghdad, Iraq

## Article Info

## ABSTRACT

A visualizing temporal stack of synthetic aperture radar (SAR) images are presented in this work, the method is called REACTIV, which enabled us to highlight color zones that have undergone change over the detected period of time. This work has been widely tested using Google earth engine (GEE) platform, this method depends on the hue-saturation-value (HSV) of visualizing space and supports estimation only in the time domain; the method does not support the spatial estimation. The coefficient of temporal coefficient variation is coded depending on the saturation color, of which several statistical properties are described. The limitations are studied, and some applications are implemented in this study.
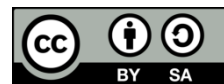
*Corresponding Author:*

Raad Farhood Chisab
Department of Electrical Techniques, Technical Institute-kut, Middle Technical University
Baghdad, Iraq
Email: raadfarhood@yahoo.com, raad.farhood@mtu.edu.iq

## 1. INTRODUCTION

Later 2014, following the success of European Space Agency (ESA) Copernicus acquisition programs with open-source product development, remote sensing processes and the search for new potential applications has been an unprecedented success [1]. Among the potentialities offered by this change of context, the exploitation of the temporal axis in particular is found where once obtaining a temporal series of images on the same site was rare and difficult [2], today many download platforms make it possible to build such batteries very quickly and anywhere in the world [3]. In parallel with obtaining these data, solutions for treating them with large computing powers are developing [4]. Synthetic aperture radar (SAR) images have remarkable temporal properties: as the images do not suffer from cloud cover, and the radar is an active system, the signal is stable between two acquisitions under interferometric conditions [5]. Also, among the advantages of having long time series, one finds in particular the fact to improve the quality, by simple temporal filtering, or by more evolved methods, but also the detection of change or more largely, the follow-up of activity. In return, the SAR images, by their coherent nature, are subject to the speckle phenomenon [6].

The binary detection principle is shown when testing change detection where modified areas are looked for between two dates. Even before the change detection decision, having a visualization method of the images highlighting this information is useful for an operator [7]. Conventionally, the visualization of a change detection scenario involves the use of complementary colored channels (green/magenta, red/cyan, or yellow/blue). The two channels encode the respective intensities of the images of the couple. As a result, the presence of different behaviors between two image's results in color, while the pixels of a stable amplitude

will appear in gray levels [8], this method can be extrapolated to the case of the only three images, since the red, green, and blue (RGB) space is three-dimensional. But for N>3 images, the visualization of the changes is not so immediate anymore. It is possible to go through animations, as in [9] which make it possible to differentiate the permanent type changes from those which are occasional changes, but these products remain video objects [10], which do not address the problem of temporal reduction, allowing the result of a single product summarizing all the changes that have occurred [11].

In this paper, we seek to find such a representation based on colored composition and that exploits at best the time axis for activity monitoring. Several works in the literature propose color compositions that use the interferometric coherence information of a temporal stack. Among them, Akbari *et al.* [12] proposes such an approach called multi temporal change (MTC) for the visualization of lava extension zones. Red and green channels encode amplitude images of the interferometric pair and the blue channel the level of interferometric coherence. This color composition does not really address the reduction of the temporal dimension [13]. Simply recommend choosing the pair minimizing both the temporal and geometric baseline.

In the same way, research [14] shows several RGB color compositions where coded channels are either an amplitude or a coherence calculated on a Sentinel-1 interferometric pair at 12, 24 and 48 days of time baselines. Other colored compositions simply use as input images of three interferometric coherence. Liao *et al.* [15] proposes a representation called CovAmCoh, again allowing visualizing changes on a pair of images under interferometric conditions. Coding of the red channel is doing by using coefficient of variation of SAR; here it is the spatial coefficient of variation, and not the temporal one, this parameter then gives information on the local heterogeneity [16]. As two images are considered, it is possible to average the two locally calculated coefficients of variation maps. The green channel encodes the amplitude, and the blue channel encodes the interferometric coherence. All these compositions only illustrate the relevance of the information contained in the level of interferometric coherence [17].

The first works that really address the use of the temporal dimension are presented in [18]. The authors propose, in a first product called level $1\alpha$, to separate the intensities related to the dry season coded in blue, those linked to the wet season, coded in green. Finally, the red channel encodes the interferometric coherence, which makes it possible to bring out in this color the anthropoid targets. Colin-Koeniguer *et al.* [18] propose a RGB visualization product called level $1\beta$, "superior" in the sense that it involves in the coding a temporal statistical parameter which is that of the variance of intensities. Red encodes this variance, the green channel encodes the average intensity, and finally the blue channel is a combination of the average interferometric coherence and a coefficient proportional to the intensity. The latter product $1\beta$ therefore uses the notion of temporal variance. More recently, Office National d'Etudes et Recherches Aérospatiales (ONERA) proposed a colored representation of temporal stacks of SAR data [19]. This representation is intended to make appear in color the pixels which are the seat of potential changes, and to leave in grayscale pixels unchanged.

This approach differs from previous studies on at least three criteria: the first of which is that a crucial temporal parameter used is the temporal coefficient of variation, which has remarkable statistical properties. No spatial estimate is made in the composition. The second of which is that the color composition passes through the use of the hue-saturation-value (HSV) color representation space before being converted into the conventional RGB space. Finally, it only uses, at the input, the amplitude, and can therefore be tested on georeferenced data of the Sentinel-1 ground range detected (GRD) type.

In this article, ambition is twofold. First of all, it is necessary to explain the temporal statistical properties of the criterion used in this approach and which partially explain its efficiency; the next step is to analyze the results on a global scale, following the implementation of the method on the Google earth engine (GEE) platform. This implementation of work is an opportunity to make a return experience of this platform. The article is structured, in section 2, the proposed principle of visualization is presented, this work addresses the theoretical statistical framework for modeling the coefficient of variation useful for visualization. In section 3, these results make it possible both to better understand the effectiveness of the method and manage its settings. The limits and potential improvements to the GEE platform are discussed and several types of results are analyzed, from which different potential applications result. Finally, in section 4, a conclusion allows us to summarize the main results obtained and to discuss the prospects for change.

## 2. THE PROPOSED ALGORITHM

This section, it is explaining the general principle of the method, to switch to the HSV color space, where the hue of the H channel is representative of the time, the saturation channel S is used to highlight the colors where the change is significant, and the value V corresponds to a notion of classic radar intensity. For this reason, our visualization method is called REACTIV for fast variation and detection in radar time-series with the use of the factor of variation. In practice, several choices are possible to have color association by a specific time agreeing to the change that one wishes to highlight [20]. Indeed, for N dates, several types of

temporal events can be considered as changes: the punctual appearance of an object (a vehicle), an appearance or permanent disappearance (the construction or the destruction of a building), or more complex events such as seasonal variations on plant parcels. Given the diversity of these situations, there is no single coding solution, but several solutions to adapt to the types of events to highlight or not [21].

Visualization method REACTIV uses intensity (V-channel) the image of maximum intensity: this maximizes the chances of seeing the event whatever it is. For hue, a color is associated with the date for which the maximum intensity is reached. This choice will be particularly suitable for a punctual event (the presence of a boat). In the case of a permanent appearance, the color will be representative of the date when the signal will be maximum; it will not necessarily be the date of the appearance of the object, but one of the dates at which it is particularly "strong" [22].

In the case of permanent destruction, the date will belong to one of the dates when the object was visible. It is possible to use in the intensity channel, an average of the images of the stack, in order to benefit at the same time of a speckle filtering [23]. However, in this case, all changes of a one-off nature disappear rapidly, visualization will above all allow to see the seats of seasonal or persistent phenomena. Finally, a saturation could be coded with a factor of temporal variation whose interest is to react to the presence of changes. Thus, the saturation of the color will be all the stronger as the temporal signal attached to a pixel will have a specific temporal evolution [24].

## 2.1. Dynamic settings

In order to debug the color coding, the actual parameters used for visualization must be defined between 0 and 1 [25]. Here, the choices made on the hue and value parameter are explained. The remaining choice, relative to the coefficient of variation, is based on the analysis of the statistical properties of this parameter [26].

H hue: the colored composition affects a color on a specific date. Built-in batteries are not necessarily acquired with regular time sampling [27]: when an acquisition is missing from the stack, it causes a jump in acquisition dates. Also, our choice is to set the date linearly with respect to the chosen acquisition range [28]. If *t1* and *t2* are starting, and end dates of the stack, that are going to be displayed, then each image acquisition date *t* is recovered for, in order to calculate the time fraction $ft$, as shown as in the (1).

$$ft = \frac{t - t1}{t2 - t1} \tag{1}$$

This parameter is a real between 0 and 1, it serves directly to code as it is the channel H of the image hue, also it should be noted in this composition, that the first and the last date have very similar colors because the HSV color palette is continuous and loop on itself [29].

The intensity (V): the intensity is coded by the maximum amplitude channel. If there is no change, and the temporal periodicity is respected, then this intensity follows a classical law gamma order L [28]. Also, the dynamics' choices made can be done in a conventional way in radar imaging thresholding the image on a maximum value of dynamics [30]. For visualization purposes, the values stored in dB were converted into linear amplitude levels, then threshold the dynamics to 1 (0 dB) and applied a contrast factor or gamma parameter equal to 1:3.

## 2.2. Dynamics of the coefficient of variation: theoretical aspects

The originality of the REACTIV composition lies mainly in the use of the temporal variation coefficient to calculate the saturation parameter. It is this parameter that will or will not make our eye interpret the color as related to a change. This section is interested in the statistical properties of this coefficient that allow to the better understanding its behavior.

### 2.2.1. Coefficient of variation of a speckle area

In radar images, it is generally believed when the amplitude of a texture less speckle which follow the law of a Rayleigh-Nakagami law [31], as the (2):

$$RN[\mu, L](\mu) = \frac{2}{\mu} \frac{\sqrt{L}}{\Gamma(L)} \left(\frac{\sqrt{L}u}{\mu}\right)^{2L-1} e^{-\left(\frac{\sqrt{L}}{\mu}u\right)^2} \tag{2}$$

where μ is a shape parameter and L is what is called the number of equivalent looks. Commonly, the law used will make estimation spatially on similar zone. This work focuses on the statistics of time. Also, assuming that for any pixel which belong to a Rayleigh Nakagami law speckle zone has not been undertaken for any variation, the numerous realizations of the amplitudes over a time of a pixel follow the same law.

This amount [32] to transforming the hypothesis of spatial periodicity into a hypothesis of temporal periodicity. In particular, as in (3):

$$m_1 = \mu \frac{\Gamma(L+\frac{1}{2})}{\sqrt{L}\Gamma(L)} \, et \, m_2 = \mu^2 \tag{3}$$

This allows to find the coefficient of variation, which is the ratio of the standard deviation and the average as in (4):

$$\gamma = \frac{\sigma}{\mu} = \frac{\sqrt{m_2 - m_1^2}}{m_1} = \sqrt{\frac{\Gamma(L)\Gamma(L+1)}{\Gamma(L+1/2)^2} - 1} \tag{4}$$

Equations here demonstrated the truth: For every average, the amplitude of the speckle, factor of the variation value could be similar for all the stable zones. So as to estimate this parameter behaves, currently the study in the change of the estimator is one of the important goals. Kendall [33] suggest calculating the difference of a function g ($m_1$, $m_2$), this can be done by a first order limited extending of the role about $m_{0,1}$ and $m_{0,2}$. The process leads to find this formula, proposed in [32]:

$$var(\gamma) = \frac{1}{4N} \frac{4m_2^3 - m_2^2 m_1^2 + m_1^2 m_4 - 4m_1 m_2 m_3}{m_1^4 (m_2 - m_1^2)} \tag{5}$$

where N is the amount of temporal pictures which is measured, showing the periods 1 to 4 of a Nakagami law, in this way the change in estimation such as L shown in (6):

$$var(\gamma) = \frac{1}{4N} \frac{L\Gamma(L)^4 (4L^2\Gamma(L)^2 - 4L\Gamma\left(L+\frac{1}{2}\right)^2 - \Gamma\left(L+\frac{1}{2}\right)^2)}{\Gamma(L+1/2)^4 (L\Gamma(L)^2 - \Gamma\left(L+\frac{1}{2}\right)^2)} \tag{6}$$

In this method where L=1, also ⅄≈0. 522723 taken var (⅄)≈0. 137881/N, (⅄)≈0. 3713/√N respectively for changes and regular deviancy. Applying a multi-look on a SAR image variation the L parameter. Sentinel-1 GRD data is provided with a number of the same looks presented at L=4.9, computed for the theoretical swath and mid-orbit value [34]. This value of L gives for the coefficient of variation associated with the speckle ⅄=0.2286, var (⅄)=0. 0216/N and (⅄)=0.1616/√N.

The equation presented another superior featured of level: 1, this equation also proved that the relationship between $\upsilon(\gamma)$ and N is inverse since $\frac{1}{\sqrt{N}}$, therefore it demonstrates that factor of variation should have a constant value through a difference reducing the square root of the number of pictures in the stack. Several simulations carried out show that when the, $\upsilon(\gamma)$ was computed on the amplitude following to a Rayleigh Nakagami law, this lead to return back to the truth of a law of Rayleigh Nakagami. The featured is very important to simulate many analyzing results and discussions [35].

### 2.2.2. Coefficient of variation of a speckle profile with temporal rupture

After having analyzed properties of the coefficient of variation for zones of pure speckle, this work proposes to simulate the way in which this coefficient behaves on a speckle zone which has a temporal rupture. This simulation is performed: It was set a number N of temporal samples, then generate $10^6$ profiles of size N, following a Rayleigh Nakagami law of parameter μ=0.3 (-11 dB) and L=4.9. the same number of profiles are also generated for which the last value of the profile is replace by fixed amplitude, considering scaled magnitudes values between $m_1$+2.5 dB and $m_1$+20 dB, representative of a longer temporal rupture. Then these realizations make it possible to calculate a coefficient of variation unique, both for pure speckle and for a temporal break [36].

This estimate is made for all the N's ranging from 2 to 200 as shown in Figure 1. The value curve (⅄+⅄) also superimposed on curves, for having an idea of the statistical distance margin between the pure speckle and temporal rupture. It is found that the coefficient variation of the pure speckle converges in function from N to the expected theoretical value (0.22), and for the other targets converges more or less rapidly towards values which are a function of the ratio between the amplitude of the target and that of speckle. Position of maximum value between the coefficient of variation of population with rupture and that without rupture depends on both N and the relative amplitude target/speckle. A remarkable result is that these curves do not depend on the average value of the speckle: with a fixed number of images, the coefficient of variation, in the presence of a temporal rupture, depends only on the jump of rupture between the speckle and the target, it deviates rapidly from the value of the coefficient of variation of a stable speckle [37].
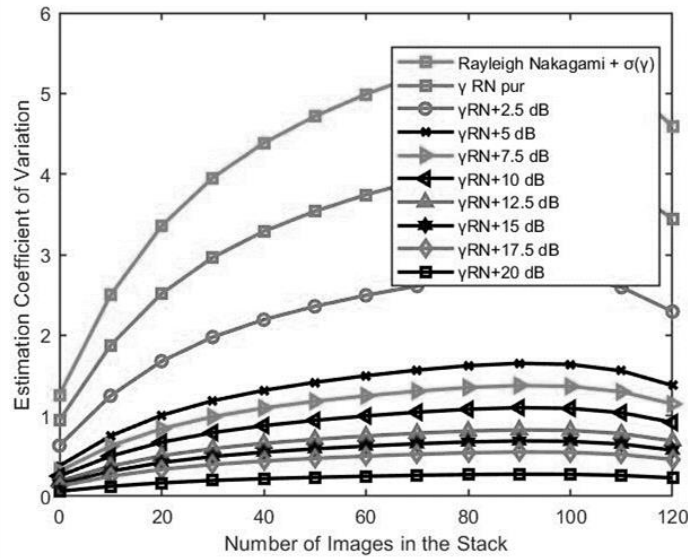
Figure 1. Simulated statistics of the coefficient of variation on a "stable"+ speckle type profile + temporary temporal rupture

## 2.3. The standardization choices

Locally, the number of images available in the same area varies, to avoid depending on $\upsilon(\gamma)$ on the number of pictures, it is necessary the normalization distribute with the help of averages [38], and the theoretical standard deviations. The statistical law of the coefficient of variation, supposed Nakagami on speckle will be approximated by normal law. A normal law does not allow overcoming the dissymmetry characteristic of Nakagami law, but to go through this approximation allows us to have a form of first-order empirical normalization by the number N [39]. In this context, the following empirical standardization shown in the (7) is proposed:

$$\gamma \leftarrow \frac{\gamma - \mu}{10\sigma} + 0.25 \tag{7}$$

A theoretic mean of typical value deviancy of "constant" speckle with L=4.9 as demonstrated in 2.2.1 this empirical standardization aims, as shown in Figure 2. A saturation of constant areas is decreased nearby of 0.25 and spreading the variations to greater saturation.
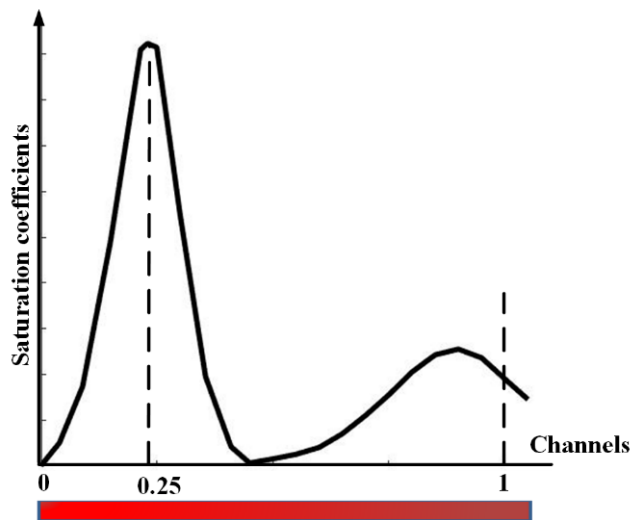


Figure 2. Empirical normalization of the saturation coefficient

## 3. RESULTS AND DISCUSSION

### 3.1. The results obtained locally and on the platform

GEE is an online platform for digital terrestrial data processing [40]. Its advantage is to store the petabytes of data collected by satellites accessible in open source. Then it makes it possible to implement and test treatments through a development interface (JavaScript API) and visualize the results on a global scale, benefiting from all the computing power of Google. The REACTIV method has been implemented on the platform to be applied to Sentinel-1 data, to demonstrate the value of visualization around the globe, and to better understand the limitations of the platform. Our approach consisted in comparing on the same area, the results obtained on the platform with those obtained with datasets downloaded and processed locally.

The study area that has been selected is Saclay in Ile de France. The Sentinel-1 GRD batteries were downloaded from the ESA platform. Then the data was pre-processed with sentinel application platform (SNAP) software, then refined the image registration with the GeFolki algorithm [41], and finally applied the REACTIV method implemented in the MATLAB language.

The stack consisted of 57 images of descending passes, acquired between 29-01-2016 and 04-04-2017, with a constant average incidence. Figure 3 shows both the representation obtained on the platform, and that obtained locally on downloaded data, for the vertical transmit and horizontal receive (VH) polarization. Visually, the representations do not seem to differ. They let appear the parcels cultivated with strongly saturated colors, as well as locally, zones of construction of which could be verified that they corresponded effectively to building sites set up at this time.
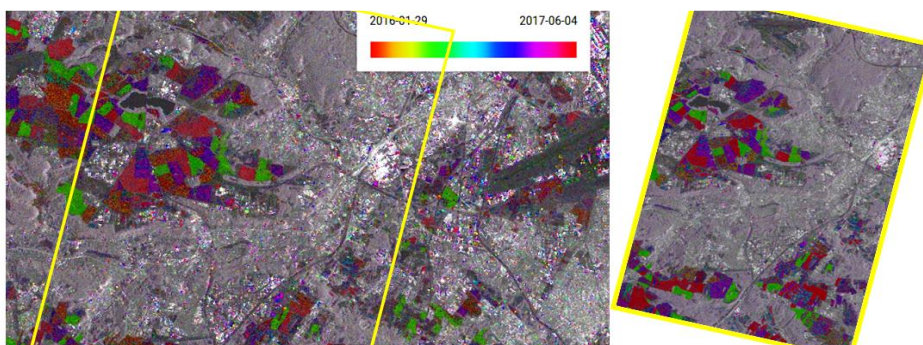


Figure 3. A zoom on a representation made from the data of the platform and the data downloaded locally, then flunked

### 3.2. The results obtained: quality registration of statistical dynamics

Today, on the platform, only georeferenced GRD-type Sentinel-1 data is available. Single look complex (SLC) data from Sentinel-1 cannot currently be embedded because earth engine does not support images with complex values because of its inability to compute them during the pyramid decomposition of images without losing the information of phases. Each GRD scene included in GEE has pretreated with SNAP by performing thermal noise suppression, radiometric calibration, and terrain correction performed with the shuttle radar topography mission (SRTM) digital elevation model (DEM) 30 or advanced spaceborne thermal emission and reflection radiometer (ASTER) DEM for areas greater than 60 degrees of latitude. No radiometric correction related to relief is currently provided.

Then the values of the geometrically corrected images are converted to decibels via logarithmic scaling. In order to save memory space, the platform makes the choice to convert float32 values to unsigned integers of 2 bytes uint16, and only retains the values between the 1st and the 99th average percentile of the values before applying the quantification. This may have the consequence of modifying the original statistics of SAR signals. Calibration of the temporal data of the platform and local data verified by the method proposed in [42]. It did not bring a substantial gain to the stability of our images, so the radiometric calibration based on metadata was kept. We analyzed the statistical distributions of the coefficient of variation for different homogeneous areas selected the image. Note that in this case, which allows us to look at the distribution of this parameter are spatial samples, even though the parameter has been calculated only temporally. The histogram of the estimated coefficient of variation on the local data is shown in Figure 4, for an area that appears to belong to a "stable" speckle zone (wooded area). In this case, the distribution seems to be well modeled empirically by a law of Rayleigh Nakagami, whose expectation and calculated standard deviation.
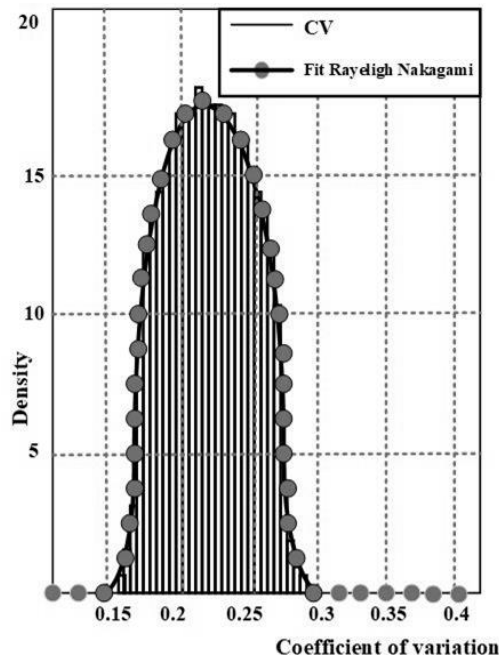
Figure 4. Local statistics of coefficient of variation on a "stable" speckle zone

By maximum likelihood are respectively equal to $\lambda$=0. 21648 and ($\lambda$)=0. 0214, values close to the theoretical values found in section 2.2, respectively 0.2286 and 0.0212. A hypothesis test with Rayleigh Nakagami law of these parameters concludes the adequacy of this law. The same estimates conducted on GEE give an average of 0.1992 and 0.0200, which provides slightly biased estimates compared to those of locally processed data. The statistical analysis was reproduced of three change-speckle zones, selected from plots of different colors in Figure 3.

For these three fields, the average values found for the coefficient of variation change between 0.3 and 0.4, and the standard deviations between 0.03 and 0.05. According to hypothesis tests put in place, the distributions obtained no longer follow the Rayleigh Nakagami law. In summary, locally statistical analysis shows that the coefficient of variation in a zone without change follows a Rayleigh Nakagami law with theoretical the values found. On the platform, the estimation results are slightly biased, although first-order errors are negligible in estimating the coefficient of variation: it is mainly the statistics on permanent broadcasters, whose values are in the distribution queue, which will be affected. It should be kept in mind that the current choice of a dynamic compression of the platform can affect quantitative results based on the statistics, even if qualitatively, visualization is not affected.

Whether on the platform or locally, the data is georeferenced using SNAP, which ensures their matching. However, the accuracy of the result obtained can be further improved. On the locally downloaded data, a sub-pixel registration method, which has the necessary accuracies for the interferometric mode, has been applied [41]. It leads to finding shifts from one image to another not insignificant, up to 2 pixels, with a standard deviation of distance found of 0.4 pixels, these residual offset can have a significant influence on the saturation and the hue obtained in the composition, especially around elements high lights: an offset on a fixed target may result in a change in the edges of the same target, at the same time, the date of a one-time event found can also be changed. Figure 5 show the effects were illustrating on a zoom which made on the site of Saclay, where several diffusers surrounded by a colored halo.

## 3.3. The results obtained of dynamic applications practices around the world

While keeping in mind the limitations of the platform, mainly related to the imperfections of georeferencing, it allows anyway to analyze very quickly the results obtained anywhere on the planet. Although it is intended to highlight the targets appearing punctually. It is seen on the example of Saclay that the color composition also allowed to visualize other types of changes, such as agricultural dynamics, and construction or destruction of urban elements. These two themes are therefore addressed, before addressing the detection of boats.

One of the first observations concerning color visualization is the marked saturation of colors on all agricultural parcels. In fact, this dynamic can give complementary information to traditional optical data. It is

therefore likely that this type of visualization adds value to the classification of agricultural parcels. This result is generalized to the entire planet explored: all agricultural parcels appear with much higher temporal variation coefficients than forest patches, for which seasonal effects are much lower.

In addition to the presence of cultivated agricultural parcels, the composition colored makes it possible to put forward building constructions. This has already been validated on the Saclay site. Another example is given in Figure 6, which shows the evolution of a district of Beijing during the year 2017.

Many colorful spots appearing in the image reflect frequent changes in land use. On a large scale, it becomes possible to map all urban areas undergoing rapid development. In the same way, it is conceivable to study the traction of structures. In Figure 7, the result of REACTIV representation applied to the city of Palmyra in Syria is an example. It shows a large number of modifications, probably related to the destruction in 2015 following the capture of the city by the Islamic State.
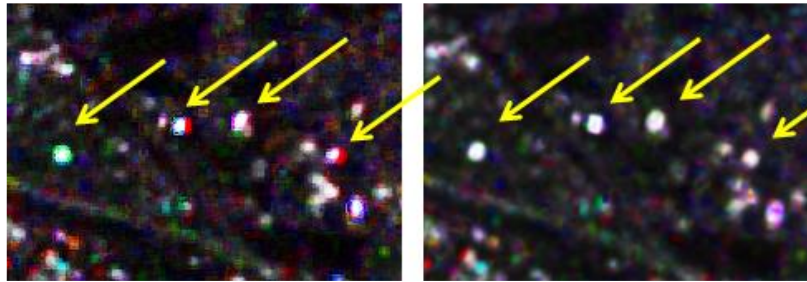


Figure 5. Zoom on a representation made on the data of the platform on the left, and data downloaded and recalibrated on the right
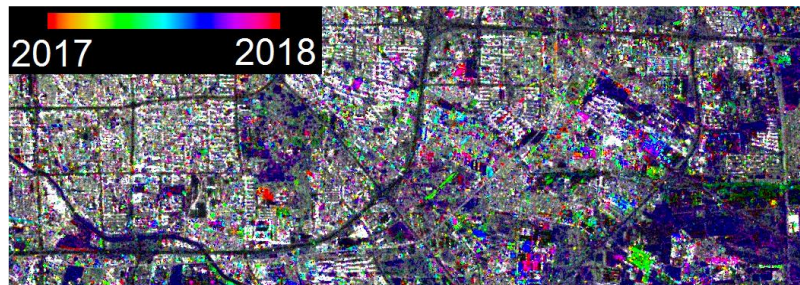


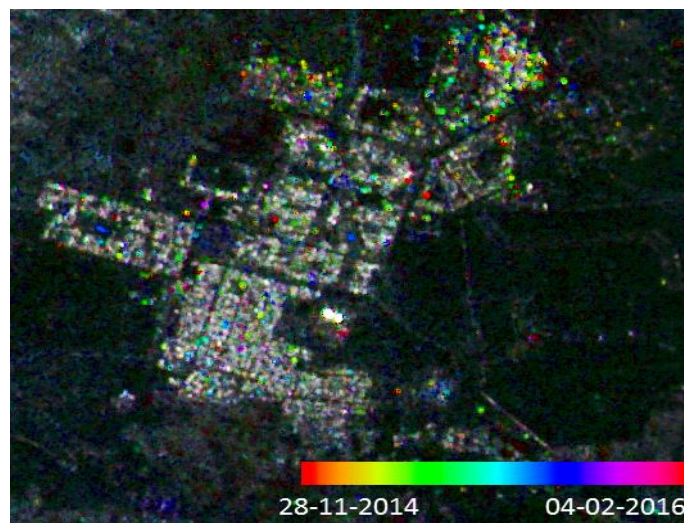Figure 6. East of Beijing, China, year 2017



Figure 7. The REACTIV composition at the palmyra site, 2015

For maritime traffic, the REACTIV visualization is particularly sensitive to targets that appear in a timely manner, it allows to identify very quickly all the boats of sufficient size, in all the port and coastal areas. In Figure 8, the products obtained around the Singapore port area, for which maritime transport is particularly important in the world, are visualized. Also, the temporal visualization makes it possible to put forward at the same time, the accumulations of boats on the zones of expectations, but also the maritime routes. Given this visualization, it is possible to perform on the ocean s' zones, temporal detection based on the use of the coefficient of variation, with a threshold positioned at the theoretical average value plus the standard deviation $0.22+0\ 1616/\sqrt{N}$. The fact of going through a temporal detection only and not space, makes it a particularly fast tool. The spatially averaged detection map in Figure 8 was obtained over the entire Sentinel-1 acquisition period (from the end of 2014 to the end of 2017) in a few seconds, to obtain a map that can be interpreted in terms of density traffic over this period.
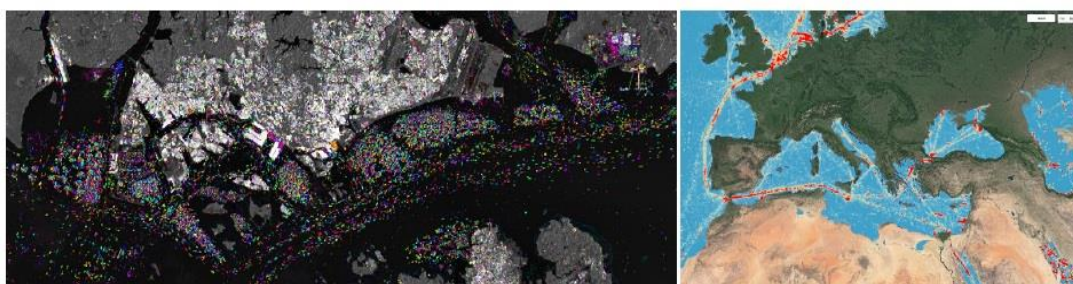


Figure 8. The REACTIV composition in Singapore from 2015 to the end of 2017 on the left, and the density map of boats detected on the right in Europe

## 4.     CONCLUSION

In this article, a REACTIV color composition, based on a coding of information in the HSV plane have been proposed, in order to optimize the analysis of a large SAR time series and in particular to address the problem of detection of changes. Temporal coefficient of variation whose statistical properties have been studied in the framework of Nakagami law achievements. It has been shown that, a speckle zone, this coefficient has a constant mean value which depends only on L, a number of equivalent looks, and that its variance decreases with the square of the number of images. A time lapse in speckle profile will result in an increase in the average value of this coefficient. The method has been implemented under the GEE platform, whose main limitations concern dynamic compression and the perfectible quality of the default registration of GRD data, the impact of which will have to be measured. Finally, on a global scale, it has been introduced visualization products for different applications that have demonstrated the effectiveness of the method. These promising results lead researchers today to consider switching from visualization to the actual detection of changes. Another challenge will be to manage the multi-event context, that is to say, to have an ability to detect several changes over time in one place.

## REFERENCES

[1]   M. S. R. Bashri and N. A. Ramli, "Flexible milimeter-wave microstrip patch antenna array for wearable RF energy harvesting applications," *International Journal of Electrical and Computer Engineering (IJECE)*, vol. 11, no. 3, pp. 1976–1984, Jun. 2021, doi: 10.11591/ijece.v11i3.pp1976-1984.

[2]   M. Ikram, M. S. Sharawi, A. Shamim, and A. Sebak, "A multiband dual-standard MIMO antenna system based on monopoles (4G) and connected slots (5G) for future smart phones," *Microwave and Optical Technology Letters*, vol. 60, no. 6, pp. 1468–1476, Jun. 2018, doi: 10.1002/mop.31180.

[3]   E. Ashraf, A. A. M. Khalaf, and S. M. Hassan, "Real time FPGA implemnation of SAR radar reconstruction system based on adaptive OMP compressive sensing," *Indonesian Journal of Electrical Engineering and Computer Science*, vol. 20, no. 1, pp. 185–196, Oct. 2020, doi: 10.11591/ijeecs.v20.i1.pp185-196.

[4]   H. Shehab, W. Ismail, and M. Singh, "Low power FSK detection at low probability bit-errors," in *2008 International Conference on Electronic Design*, Dec. 2008, pp. 1–4, doi: 10.1109/ICED.2008.4786760.

[5]   Q. Chen *et al.*, "Single ring slot-based antennas for metal-rimmed 4G/5G smartphones," *IEEE Transactions on Antennas and Propagation*, vol. 67, no. 3, pp. 1476–1487, Mar. 2019, doi: 10.1109/TAP.2018.2883686.

[6]   R. A. K. Noaman, M. A. Mohd Ali, N. Zainal, and F. Saeed, "Human detection framework for automated surveillance systems," *International Journal of Electrical and Computer Engineering (IJECE)*, vol. 6, no. 2, pp. 877–886, Apr. 2016, doi: 10.11591/ijece.v6i2.pp877-886.

[7]   D. Monica and A. Widipaminto, "Fuzzy transform for high-resolution satellite images compression," *Telecommunication

*Computing Electronics and Control (TELKOMNIKA)*, vol. 18, no. 2, pp. 1130–1136, Apr. 2020, doi: 10.12928/telkomnika.v18i2.14903.

[8]  E. Colin Koeniguer and J.-M. Nicolas, "Change detection based on the coefficient of variation in SAR time-series of urban areas," *Remote Sensing*, vol. 12, no. 13, p. 2089, Jun. 2020, doi: 10.3390/rs12132089.

[9]  C. Le Van, G. N. Nguyen, T. H. Nguyen, T. S. Nguyen, and D.-N. Le, "An effective RGB color selection for complex 3D object structure in scene graph systems," *International Journal of Electrical and Computer Engineering (IJECE)*, vol. 10, no. 6, pp. 5951–5964, Dec. 2020, doi: 10.11591/ijece.v10i6.pp5951-5964.

[10] A. Khabba, S. Ibnyaich, and M. M. Hassani, "A new design of multi-band antenna array for 5G cellular phones applications," in *2019 International Conference of Computer Science and Renewable Energies (ICCSRE)*, Jul. 2019, pp. 1–5, doi: 10.1109/ICCSRE.2019.8807553.

[11] P. Boccardo, V. Gentile, F. G. Tonolo, D. Grandoni, and M. Vassileva, "Multitemporal SAR coherence analysis: Lava flow monitoring case study," in *2015 IEEE International Geoscience and Remote Sensing Symposium (IGARSS)*, Jul. 2015, pp. 2699–2702, doi: 10.1109/IGARSS.2015.7326370.

[12] V. Akbari, S. N. Anfinsen, A. P. Doulgeris, T. Eltoft, G. Moser, and S. B. Serpico, "Polarimetric SAR change detection with the complex hotelling-lawley trace statistic," *IEEE Transactions on Geoscience and Remote Sensing*, vol. 54, no. 7, pp. 3953–3966, Jul. 2016, doi: 10.1109/TGRS.2016.2532320.

[13] U. Wegmüller, M. Santoro, C. Werner, and O. Cartus, "On the estimation and interpretation of Sentinel-1 TOPS InSAR coherence," in *Proc' Fringe Workshop*, Frascati 2015. Italy: ESA, May 2015, doi: 10.5270/Fringe2015.pp89.

[14] K. Schulz, E. Cadario, M. Boldt, and A. Thiele, "Improving high-resolution repeat pass SAR image interpretation by the CoVAmCoh method," in *8th European Conference on Synthetic Aperture Radar*, 2010, pp. 1–4.

[15] M. Liao, L. Jiang, H. Lin, B. Huang, and J. Gong, "Urban change detection based on coherence and intensity characteristics of SAR imagery," *Photogrammetric Engineering and Remote Sensing*, vol. 74, no. 8, pp. 999–1006, Aug. 2008, doi: 10.14358/PERS.74.8.999.

[16] D. B. Taha, T. B. Taha, and N. B. Al Dabagh, "A comparison between the performance of DWT and LWT in image watermarking," *Bulletin of Electrical Engineering and Informatics*, vol. 9, no. 3, pp. 1005–1014, Jun. 2020, doi: 10.11591/eei.v9i3.1754.

[17] D. Amitrano, G. Di Martino, A. Iodice, D. Riccio, and G. Ruello, "RGB SAR product exploiting multitemporal: General processing and applications," in *2017 9th International Workshop on the Analysis of Multitemporal Remote Sensing Images (MultiTemp)*, Jun. 2017, pp. 1–4, doi: 10.1109/Multi-Temp.2017.8035221.

[18] E. Colin-Koeniguer, A. Boulch, P. Trouve-Peloux, and F. Janez, "Colored visualization of multitemporal SAR data for change detection: issues and methods," in *EUSAR 2018-12th European Conference on Synthetic Aperture Radar*, 2018, pp. 1–4.

[19] A. M. Atto, E. Trouve, Y. Berthoumieu, and G. Mercier, "Multidate divergence matrices for the analysis of SAR image time series," *IEEE Transactions on Geoscience and Remote Sensing*, vol. 51, no. 4, pp. 1922–1938, Apr. 2013, doi: 10.1109/TGRS.2012.2210228.

[20] R. Caye Daudt, B. Le Saux, and A. Boulch, "Fully convolutional siamese networks for change detection," in *2018 25th IEEE International Conference on Image Processing (ICIP)*, Oct. 2018, pp. 4063–4067, doi: 10.1109/ICIP.2018.8451652.

[21] E. B. Candrasari, L. Novamizanti, and S. Aulia, "Hand gesture recognition using discrete wavelet transform and hidden Markov models," *Telecommunication Computing Electronics and Control (TELKOMNIKA)*, vol. 18, no. 5, pp. 2265–2275, Oct. 2020, doi: 10.12928/telkomnika.v18i5.13725.

[22] B. Zong *et al.*, "Deep autoencoding gaussian mixture model for unsupervised anomaly detection," In *Proceedings of the 6th International Conference on Learning Representations*, Vancouver, BC, Canada, 2018.

[23] A. Bhowmik, J. Dey, A. Sarkar, and S. Karforma, "Computational intelligence based lossless regeneration (CILR) of blocked gingivitis intraoral image transportation," *IAES International Journal of Artificial Intelligence (IJ-AI)*, vol. 8, no. 3, pp. 197–204, Dec. 2019, doi: 10.11591/ijai.v8.i3.pp197-204.

[24] A. K. Mishra and R. Pandey, "A review on modelling and performance of QAM-OFDM system with AWGN channel," *International Journal of Emerging Technology and Advanced Engineering*, vol. 4, no. 3, pp. 649–652, 2014.

[25] D. Amitrano, G. Di Martino, A. Iodice, D. Riccio, and G. Ruello, "An end-user-oriented framework for the classification of multitemporal SAR images," *International Journal of Remote Sensing*, vol. 37, no. 1, pp. 248–261, Jan. 2016, doi: 10.1080/01431161.2015.1125550.

[26] R. F. Chisab and C. K. Shukla, "The downlink 4G-LTE in fading channel based on the multiwavelet transform," in *2014 International Conference on Computational Intelligence and Communication Networks*, Nov. 2014, pp. 233–236, doi: 10.1109/CICN.2014.61.

[27] M. F. E. Purnomo *et al.*, "Development of patch stack antenna for CP-SAR sensor," *Bulletin of Electrical Engineering and Informatics*, vol. 10, no. 1, pp. 200–207, Feb. 2021, doi: 10.11591/eei.v10i1.2672.

[28] C. Zhou and R. C. Paffenroth, "Anomaly detection with robust deep autoencoders," in *Proceedings of the 23rd ACM SIGKDD International Conference on Knowledge Discovery and Data Mining*, Aug. 2017, pp. 665–674, doi: 10.1145/3097983.3098052.

[29] M. Priyatharishini and M. N. Devi, "A compressive sensing algorithm for hardware trojan detection," *International Journal of Electrical and Computer Engineering (IJECE)*, vol. 9, no. 5, pp. 4035–4043, Oct. 2019, doi: 10.11591/ijece.v9i5.pp4035-4043.

[30] C. Periyasamy, "Satellite image enhancement using dual tree complex wavelet transform," *Bulletin of Electrical Engineering and Informatics*, vol. 6, no. 4, pp. 334–336, Dec. 2017, doi: 10.11591/eei.v6i4.861.

[31] J. W. Goodman, "Some fundamental properties of speckle," *Journal of the Optical Society of America*, vol. 66, no. 11, pp. 1145–1150, Nov. 1976, doi: 10.1364/JOSA.66.001145.

[32] G. Mercier, "Progressive change detection in time series of SAR images," in *2010 IEEE International Geoscience and Remote Sensing Symposium*, Jul. 2010, pp. 3086–3089, doi: 10.1109/IGARSS.2010.5652452.

[33] M. G. Kendall, *The advanced theory of statistics, Vol. 1: distribution theory*. C. Griffin; 4th ed edition, 1977.

[34] Sentinel 1 Team, *Sentinel 1 user handbook*. European Space Agency (ESA), 2013.

[35] A. Desai, R. Patel, T. Upadhyaya, H. Kaushal, and V. Dhasarathan, "Multiband inverted E and U shaped compact antenna for Digital broadcasting, wireless, and sub 6 GHz 5G applications," *AEU-International Journal of Electronics and Communications*, vol. 123, p. 153296, Aug. 2020, doi: 10.1016/j.aeue.2020.153296.

[36] M. R. Narasinga Rao, D. Gurram, S. M. Vadde, S. Tallam, N. S. Chand, and L. Kiran, "A predictive model for mining opinions of an educational database using neural networks," *International Journal of Electrical and Computer Engineering (IJECE)*, vol. 5, no. 5, pp. 1158–1163, Oct. 2015, doi: 10.11591/ijece.v5i5.pp1158-1163.

[37] M. K. Kaushik, Y. Yoganandam, and S. K. Sahoo, "Sensing and sharing schemes for spectral efficiency of cognitive radios," *International Journal of Electrical and Computer Engineering (IJECE)*, vol. 8, no. 5, pp. 2934–2941, Oct. 2018, doi: 10.11591/ijece.v8i5.pp2934-2941.

[38] A. J. Khalilabadi and A. Zadehgol, "Multiband antenna for wireless applications including GSM/UMTS/LTE and 5G bands," in *2018 International Applied Computational Electromagnetics Society Symposium (ACES)*, Mar. 2018, pp. 1–2, doi: 10.23919/ROPACES.2018.8364167.

[39] P. K. Mane and K. N. Rao, "Granular mobility-factor analysis framework for enriching occupancy sensing with doppler radar," *International Journal of Electrical and Computer Engineering (IJECE)*, vol. 8, no. 2, pp. 979–988, Apr. 2018, doi: 10.11591/ijece.v8i2.pp979-988.

[40] N. Gorelick, M. Hancher, M. Dixon, S. Ilyushchenko, D. Thau, and R. Moore, "Google Earth Engine: Planetary-scale geospatial analysis for everyone," *Remote Sensing of Environment*, vol. 202, pp. 18–27, Dec. 2017, doi: 10.1016/j.rse.2017.06.031.

[41] A. Plyer, E. Colin-Koeniguer, and F. Weissgerber, "A new coregistration algorithm for recent applications on Urban SAR images," *IEEE Geoscience and Remote Sensing Letters*, vol. 12, no. 11, pp. 2198–2202, Nov. 2015, doi: 10.1109/LGRS.2015.2455071.

[42] G. Quin, B. Pinel-Puyssegur, J.-M. Nicolas, and P. Loreaux, "MIMOSA: an automatic change detection method for SAR time series," *IEEE Transactions on Geoscience and Remote Sensing*, vol. 52, no. 9, pp. 5349–5363, Sep. 2014, doi: 10.1109/TGRS.2013.2288271.

## BIOGRAPHIES OF AUTHORS

**Hamood Shehab Hamid** received his B.Sc. in Collage of Electrical and Electronic Engineering, University of Sarajevo, 1986, Received the M.Sc., Belgrade University, 1988, Yugoslavia. He received his Ph.D. in Wireless and Mobile Communication Systems from the School of Electronic Engineering, University Sciences Malaysia (USM), Pinang-Malaysia. 2011. The author works as a lecturer, researcher, and training supervisor in the Ministry of Higher Education and Scientific Research/Middle technical University-Baghdad-Iraq and he is a faculty member at the College of Electrical and Electronic Engineering Techniques, Department of Computer Engineering Techniques. His research interest includes Wireless Mobile System Communication Engineering, Small Form Factor (SFF) Software-Defined Radio (SDR), Digital Signal Processing and Image Processing, Antenna Design, and Antennas for Medical applications. He can be contacted at email: drhamood@mtu.edu.iq.

**Raad Farhood Chisab** was born in Baghdad-Iraq in 1975. He received the B.Sc. in Electrical Engineering and M.Sc. degree in Control and Computer Engineering from College of Engineering-University of Baghdad. In 2015 the author gets his Ph.D. degree in Electronic and Communication Engineering from SHIATS University-India. From 2005 the author works as lecturer, researcher and training supervisor in the Ministry of Higher Education and Scientific Research-Middle technical University-Baghdad. His research interest includes signal processing, image processing, wireless communication, mobile technology, wireless sensor network, IOT, 4G and 5G technology. The author published about 20 papers in national and international journals. He can be contacted at email: raadfarhood@yahoo.com, raad.farhood@mtu.edu.iq.